Computational Study on Interaction Between Swimming Fish and Drifting Vortices Behind the Cylinder

TONG Ying[1,2], *XIA Jian*[1,2*], *CHEN Long*[1,2], *XUE Haotian*[1,2]

1. College of Aerospace Engineering, Nanjing University of Aeronautics and Astronautics, Nanjing 210016, P. R. China;
2. Key Laboratory of Unsteady Aerodynamics and Flow Control of Ministry of Industry and Information Technology, Nanjing University of Aeronautics and Astronautics, Nanjing 210016, P. R. China

(Received 8 August 2021; revised 23 November 2021; accepted 20 December 2021)

Abstract: To predict the flow evolution of fish swimming problems, a flow solver based on the immersed boundary lattice Boltzmann method is developed. A flexible iterative algorithm based on the framework of implicit boundary force correction is used to save the computational cost and memory, and the momentum forcing is described by a simple direct force formula without complicated integral calculation when the velocity correction at the boundary node is determined. With the presented flow solver, the hydrodynamic interaction between the fish-induced dynamic stall vortices and the incoming vortices in unsteady flow is analyzed. Numerical simulation results unveil the mechanism of fish exploiting vortices to enhance their own hydrodynamic performances. The superior swimming performances originate from the relative movement between the "merged vortex" and the locomotion of the fishtail, which is controlled by the phase difference. Formation conditions of the "merged vortex" become the key factor for fish to exploit vortices to improve their swimming performance. We further discuss the effect of the principal components of locomotion. From the results, we conclude that lateral translation plays a crucial role in propulsion while body undulation in tandem with rotation and head motion reduce the locomotor cost.

Key words: immerse boundary; lattice Boltzmann method; complex deformable boundary; fluid-fish interaction; hydrodynamic mechanism; bionic propulsion

CLC number: TN925 **Document code:** A **Article ID:** 1005-1120(2022)01-0108-13

0 Introduction

The natural characteristics of fish swimming such as high maneuverability, long endurance ability, and strong adaptability to the environment are beyond the reach of traditional underwater vehicles. These differences may be due to the excellent performances from the evolution of fish, including complex movement patterns, special epidermal characteristics, and perception of vortices in the natural environment. The hydrodynamic mechanism of fish swimming has attracted widespread attentions from researchers and engineers who try to apply these mechanisms in the design of underwater vehicles[1-4]. Exploring the mechanism of fish exploiting vortices in the natural environment to improve their hydrodynamic performance has become a central issue for improving and enhancing the propulsion and endurance capabilities of aquatic bionic vehicles[5-6].

The early research approaches on this subject are mainly theoretical analyses, including the resistive force theory[7], the reactive force theory[8], the waving plate theory[9], and the potential flow theory[10]. They are based on simple geometry and single motion patterns, and ignore the effect of fluid viscosity. From the 21st century, numerous models based on viscous incompressible fluids have been established to understand the mechanism of the interaction between the unsteady flows and various

*Corresponding author, E-mail address: jxia@nuaa.edu.cn.

How to cite this article: TONG Ying, XIA Jian, CHEN Long, et al. Computational study on interaction between swimming fish and drifting vortices behind the cylinder[J]. Transactions of Nanjing University of Aeronautics and Astronautics, 2022, 39 (1): 108-120.

http://dx.doi.org/10.16356/j.1005-1120.2022.01.011

aquatic swimmers in the natural environment. Two main simplified models of fish-like motion are rigid flapping and flexible undulatory models. The flapping model[11] was originally used to describe the aerial flights of birds and insects then extended to describe the aquatic swimming of fishes. It is a combination of pitching and heaving. Gopalkrishnan et al.[12] investigated the hydrodynamic performance of foil with the flapping model behind the D-shaped cylinder. The results showed that the incoming vortices of the *Kármán* vortex street were repositioned, and their strength changed by the flapping foil. Akhtar et al.[13] established a simplified multi-fin model using two rigid finite-thickness flat plates with the flapping motion pattern, and investigated the effect of the vortex generated by the dorsal fin vibration on the thrust and efficiency of the downstream caudal fin. Karbasian et al.[14] numerically simulated foil swimming using an improved flapping model, and the relationship between the kinematics of foil and flow structure around the foil was analyzed. The above-mentioned studies used the flapping model to describe fish-like swimming, whereas the effect of flexible bodies was not considered.

Most of the streamlined fish adopt an undulatory mode to generate propulsion. Barrett et al.[15] studied the force and power during the motion of the robotic fish in the undulatory mode of propulsion. Experimental data showed that at the same propulsive velocity, robotic fish with undulatory mode of propulsion can reduce the power consumption compared with rigid robotic fish. Beal et al.[16] studied the motion patterns of lifeless fish in a vortex wake. The results showed that the energy passively extracted by the inanimate fish from the vortex would provide greater propulsion for its own motion, which caused it to move upstream. It was concluded that fish selectively extracted energy from the incoming vortices by actively altering their own locomotion. Considering the factors affecting the optimal hydrodynamic performance, the numerical results proposed by Shao et al.[17] and Xiao et al.[5] confirmed that within certain parameter ranges, the incoming vortices increased the thrust generated by fish with a single undulatory mode of propulsion. However, these simplified models only considered the undulation, but neglected the flapping model.

For the locomotion of swimmers, it is recognized that there is no optimal motion pattern, but the combination of different motion patterns may improve the performance of swimmers. Bergmann et al.[18] proposed a model that considered coupled kinematics. Flapping and undulation motions were put into the locomotion of foil at the same time, and the effect of velocity coupling on its performance was numerically analyzed. In each time step, the locomotion of the foil consisted of active undulation and passive flapping, and the rigid flapping was determined by the Newton laws of mechanics using the hydrodynamic forces and moment acting on the fish surface. Using the coupled kinematic model, Zhu et al.[19] numerically studied the adaptive behaviors of a fully self-propelled smart swimmer in complex vortex environments. Akanyeti et al.[20] expanded a series of experimental research results of Liao et al.[21-23] and proposed a kinematic analytical model to describe the *Kármán* gait. This analytical model showed that the real locomotion of trout in the wake of D-shape cylinder was the superposition of pitching, heaving, undulation, and heading motion. Stewart et al.[24] studied the kinematics of the *Kármán* gait in the vortex wake behind the tandem cylinder, and found that the wavelength of the vortex wake and the body wavelength of the *Kármán* gait fish satisfied a linear correlation. Recently, Li et al.[6] simplified the *Kármán* gait model via the combination of heaving and undulatory motions, and the effects of flow control parameters on the hydrodynamic performance of the fish were investigated numerically.

The existing numerical models do not consider the complete locomotion of live fish in the vortex environment. The main contribution of the presented study is that the complete *Kármán* gait motion pattern is used to investigate the hydrodynamic mechanisms, which involves the pitching, heaving, undulatory, and heading motions. Additionally, the hydrodynamic interaction between the dynamic stall vortex induced by fish and the incoming flow vortex plays a key role in the hydrodynamic performance of the fish. Although numerous experimental and numerical studies have been undertaken, the focus is to understand the kind of flow control parameters that improve the hydrodynamic performance of fish. However, the relationship of the flow structure induced by the locomotion of fish and the incoming vortices is not well understood. The factors of flow pattern around the foil that influence the extraction of energy by fish from the incoming vortex have not been systematically investigated.

Using the *Kármán* gait kinematic analytical model to force the foil locomotion and place it behind the cylinder, the simulation of the fish swimming in the vortex street wake is performed based on the immersed boundary lattice Boltzmann methods (IB-LBM)[25]. Benefiting from the common features of the Cartesian grid, the lattice Boltzmann method was combined firstly with the immersed boundary[26-27] in 2004[28]. Subsequently, several improved IB-LBM have been developed[29-32]. At present, IB-LBM has been proven to be an effective numerical simulation method for simulating the flow around complex deformable bodies[33-34]. In this work, a flexible iterative algorithm is employed to improve the implicit velocity correction IB scheme, so that the deformable moving boundary can be processed based on the desirable computational cost and memory.

The rest of this paper is organized as follows. Section 1 describes the physical model. Section 2 elaborates the computational model and performance parameters. Section 3 includes the numerical results and discussion. The last section of this paper is the conclusion.

1 Physical Model

The flow that goes past a fish adopting the *Kármán* gait periodically generates a pair of alternating counter-rotating vortices from the sides of the fish head and the caudal fin. These kinematic vortices interact with the incoming vortices to create a mysterious nonlinear coupled dynamic system. As the subject of this paper, the interaction between the incoming vortex and the vortex shedding from the swimming fish is investigated using a simpler model. The flow configuration is shown in Fig.1. The NACA0012 airfoil with the chord length L is placed directly behind the cylinder with the diameter D, where $L=2D$. The distance between the center of the cylinder and the tip of the fish is equal to $2L$. Numerical results show that the cylinder-foil distance $2L$ can ensure that the vortex flow generated by the upstream cylinder remains periodicity and cannot be disturbed by the fluctuation of the downstream foil.

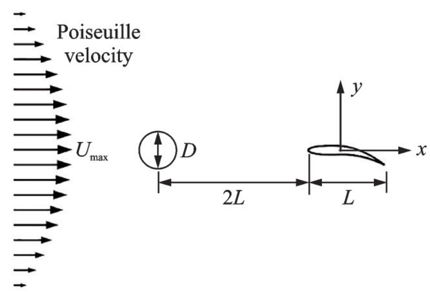

Fig.1 Flow configuration composed of a stationary cylinder and a streamlined fish

The computational domain size is $10D\times25D$. The Poiseuille velocity distribution is used as the inlet boundary condition, and the free outflow condition is set as the outlet boundary condition. The upper and lower boundaries adopt stationary wall conditions. The cylinder and the fish body employ the IB model to force the non-slip condition. The Reynolds number is calculated based on the diameter of the cylinder D, the inflow velocity U, and the fluid viscosity ν, where Re of all simulations discussed here are 100.

We use the *Kármán* gait analytical model presented by Akanyeti et al.[20] to force the foil locomotion. The parameters and traveling wave equation expressions of the analytical model are listed in Table 1. In Table 1, ϕ_0 is the phase angle of heaving motion, f is the frequency of fish vibration, and λ is the fish body wavelength, where $\lambda=1.25\lambda_{wake}$ and $f=f_{vs}$ is satisfied (λ_{wake} and f_{vs} are the cylinder wake variables). A series of instantaneous postures of fish within a kinematic cycle is shown in Fig.2. These postures agree well with the experimental results of Ref.[21].

Table 1 Description of the Kármán gait analytical model

Motion	Traveling wave equation	Extent
Translation	$0.15L_f\sin\left(2\pi ft+\phi_0\right)$	$x\in[0,\ L]$
Rotation	$(x-0.3L)\sin\left[0.135\,263\sin\left(2\pi ft+\phi_0+\pi\right)\right]$	$x\in[0,\ L]$
Undulation	$\left[0.01L\left(\frac{x}{L}-0.4\right)+0.51L\left(\frac{x}{L}-0.4\right)^2\right]\sin\left[\frac{2\pi}{\lambda}\left(\frac{x}{L}-0.4\right)-2\pi ft+\phi_0-\frac{\pi}{2}\right]$	$x\in[0.4L,\ L]$
Heading	$(x-0.2L)\sin\left[0.069\,813\sin\left(2\pi ft+\phi_0\right)\right]$	$x\in[0,\ 0.2L]$

Fig.2 Fish instantaneous posture during a kinematic cycle

2 Computational Model

2.1 Numerical method

The split-forcing scheme Lattice Boltzmann equation (LBE)[35] with the Bhatnagar-Gross-Krook (BGK) collision operator is expressed as

$$f_\alpha\left(\boldsymbol{x}+\boldsymbol{c}_\alpha\Delta t,t+\Delta t\right)=f_\alpha(\boldsymbol{x},t)-\frac{1}{\tau}\left[f_\alpha(\boldsymbol{x},t)-f_\alpha^{\mathrm{eq}}(\boldsymbol{x},t)\right]\Delta t+F_\alpha(\boldsymbol{x},t)\Delta t \tag{1}$$

where f_α is the density distribution function (DDF) along the α-direction at lattice node $\boldsymbol{x}$ and time t. The discrete velocity set $\boldsymbol{c}_\alpha$ couples time and space in the LB model. It guarantees that after Δt, the particle at the lattice node $\boldsymbol{x}$ precisely reaches the adjacent lattice node $\boldsymbol{x}+\boldsymbol{c}_\alpha\Delta t$. It has been proven that for the internal node of computational domain, the split-forcing LBE is second-order accurate in space and time[36-37]. The collision operator represents the advection of f_α, it is linear and related to the equilibrium DDF f_α^{eq}. Limiting the Hermite expansion of f_α^{eq} to the second-order, the hydrodynamics macroscopic laws can be guaranteed[38]. The expression of f_α^{eq} can be written as

$$f_\alpha^{\mathrm{eq}}=\omega_\alpha\rho\left(1+\frac{\boldsymbol{c}_\alpha\cdot\boldsymbol{u}}{c_s^2}+\frac{(\boldsymbol{c}_\alpha\cdot\boldsymbol{u})^2}{2c_s^4}-\frac{\boldsymbol{u}\cdot\boldsymbol{u}}{2c_s^2}\right) \tag{2}$$

where ω_α is the weighted coefficient associated with $\boldsymbol{c}_\alpha$. In this paper, the D2Q9 model is employed, and the details can be found in Ref. [39]. c_s is sound speed, $c_s^2=\frac{1}{3}\Delta x^2/\Delta t^2$. Δx and Δt are the lattice space size and the time step size, respectively. In the isothermal LB model, c_s^2 is the proportional coefficient between pressure p and density ρ, $p=c_s^2\rho$. In the IB-LBM environment, the discrete force distribution function F_α essentially describes the contribution from the boundary, which is a function of the momentum forcing $\boldsymbol{f}$. Like expansion of f_α^{eq}, the Hermite expansion of F_α is restricted to the second-order. Its expression is given that

$$F_\alpha=\left(1-\frac{1}{2\tau}\right)\omega_\alpha\left(\frac{\boldsymbol{c}_\alpha-\boldsymbol{u}}{c_s^2}+\frac{\boldsymbol{c}_\alpha\cdot\boldsymbol{u}\cdot\boldsymbol{c}_\alpha}{c_s^4}\right)\cdot\boldsymbol{f} \tag{3}$$

Depending on the multi-scale Chapman-Enskog expansion, the split-forcing LBE is able to recover the Navier-Stokes equations involving the momentum forcing for solving the flow problems of incompressible viscous fluid past the immersed bodies.

The macroscopic density and momentum of fluid can be calculated in a down-top manner

$$\rho=\sum_\alpha f_\alpha \tag{4}$$

$$\rho\boldsymbol{u}=\sum_\alpha\boldsymbol{c}_\alpha f_\alpha+\frac{1}{2}\boldsymbol{f}\Delta t \tag{5}$$

The kinematic viscosity of fluid, v, is denoted by the relation time τ as

$$v=c_s^2\left(\tau-\frac{\Delta t}{2}\right) \tag{6}$$

In the IB-LBM scheme, fluid particles are described by the uniform Eulerian lattice nodes $\boldsymbol{x}$, and the immersed boundary is represented by a series of Lagrangian points $\boldsymbol{X}(s,t)$. $\boldsymbol{X}$ is the location of immersed boundary. $\boldsymbol{x}$ and s are the Eulerian and Lagrangian coordinates. Transformation between the Lagrangian variables and Eulerian variables can be controlled by the Dirac delta function. A hat-function[40] is used to discrete the Dirac delta function and construct the interpolation function D. It is expressed as

$$D\left(\boldsymbol{x}_{ij}-\boldsymbol{X}(s)\right)=\frac{1}{\Delta x\Delta y}\phi\left(\frac{\boldsymbol{x}_{ij}-\boldsymbol{X}(s)}{\Delta x}\right)\phi\left(\frac{\boldsymbol{y}_{ij}-\boldsymbol{Y}(s)}{\Delta y}\right)\tag{7}$$

Inspired by Wu and Shu et al.[33-34], the velocity correction $\delta\boldsymbol{U}(\boldsymbol{X},t)$ can be used to enhance the no-slip condition and distributed into the surrounding Eulerian fluid nodes to construct $\boldsymbol{f}(\boldsymbol{x},t)$ and update $\boldsymbol{u}(\boldsymbol{x},t)$ by Eq.(5).

According to Eq.(1), the numerical computation process of implicit velocity correction can be divided into four steps: The collision, the first-forcing, the streaming, and the second-forcing. Pushing a new time step, the first three steps are to pre-calculate the density and velocity of fluid particles. Then, the fourth step is to calculate the velocity correction of fluid particles with the no-slip boundary as the constraint condition. In this work, the second-forcing step is constructed in an iterative manner based on the multi-direct force scheme[25]. The improved IB-LBM algorithm is reflected in the use of a simple and flexible sub-iteration instead of solving the linear equation, thereby reducing the computational cost[34]. The sub-iteration procedure is expressed as

$$\rho(\boldsymbol{X}(s),t)=\sum_{i,j}\rho\left(\boldsymbol{x}_{ij},t\right)D\left(\boldsymbol{x}_{ij}-\boldsymbol{X}(s)\right)\Delta x\Delta y\tag{8}$$

$$\delta\boldsymbol{U}^{(n)}(\boldsymbol{X}(s),t)=\boldsymbol{U}^{B}(\boldsymbol{X}(s),t)-\sum_{i,j}\boldsymbol{u}^{(n)}\left(\boldsymbol{x}_{ij},t\right)D\left(\boldsymbol{x}_{ij}-\boldsymbol{X}(s)\right)\Delta x\Delta y\tag{9}$$

$$\boldsymbol{F}^{(n)}(\boldsymbol{X}(s),t)=\frac{2}{\Delta t}\rho(\boldsymbol{X}(s),t)\,\delta\boldsymbol{U}^{(n)}(\boldsymbol{X}(s),t)\tag{10}$$

$$\boldsymbol{f}^{(n)}\left(\boldsymbol{x}_{ij},t\right)=\sum_{s}\boldsymbol{F}^{(n)}(\boldsymbol{X}(s),t)\,D\left(\boldsymbol{x}_{ij}-\boldsymbol{X}(s)\right)\Delta x\Delta l_s\tag{11}$$

$$\boldsymbol{u}^{(n+1)}\left(\boldsymbol{x}_{ij},t\right)=\boldsymbol{u}^{(n)}\left(\boldsymbol{x}_{ij},t\right)+\frac{\Delta t}{2\rho\left(\boldsymbol{x}_{ij},t\right)}\boldsymbol{f}^{(n)}\left(\boldsymbol{x}_{ij},t\right)\tag{12}$$

where Δl is the length of the boundary element. The iteration initial condition $\boldsymbol{u}^{(0)}=\boldsymbol{u}^{*}=\sum c_\alpha \boldsymbol{f}_\alpha/\rho$ is used in the above iteration procedure; and the superscript n indicates the number of IB iteration steps. To avoid additional computational cost, the iteration parameter ϵ is used to flexibly control the number of sub-iterations. When $\|\delta\boldsymbol{U}^{(n)}\|_\infty\leqslant\epsilon$ is satisfied, the sub-iterations process is over. Analogously, Dash et al.[41] has also established the flexible forcing non-slip constraint by involving a new iteration parameter.

The velocity correction $\delta\boldsymbol{u}$ at the Eulerian nodes can be calculated by

$$\delta\boldsymbol{u}=\boldsymbol{u}^{(n+1)}-\boldsymbol{u}^{*}\tag{13}$$

The direct-forcing formula at Eulerian nodes can be expressed as

$$\boldsymbol{f}=2\rho\delta\boldsymbol{u}/\Delta t\tag{14}$$

The hydrodynamic force $\boldsymbol{H}$ acting on the boundary element can be evaluated by Eq.(15) without complicated tensor calculations

$$\boldsymbol{H}\left(\boldsymbol{X}(s,t),t\right)=-\boldsymbol{F}(\boldsymbol{X}(s,t),t)\,\Delta x\Delta l_s\tag{15}$$

2.2 Performance parameters

The propulsion performance is quantified by the mean thrust coefficient $\bar{C}_{\mathrm{T}}$. To ensure that $\bar{C}_{\mathrm{T}}>0$ when the flow provides a propulsion contribution to the fish within a certain time range $[0, t]$, $\bar{C}_{\mathrm{T}}$ is defined as

$$\bar{C}_{\mathrm{T}}=\frac{-\frac{1}{t}\int_0^t\left(\sum_s H_x(\boldsymbol{X}(s,t),t')\right)\mathrm{d}t'}{\frac{1}{2}\rho\boldsymbol{u}_\infty^2 D}\tag{16}$$

We also quantify the energy consumption level of the fish using the mean power coefficient $\bar{C}_{\mathrm{P}}$. Similarly, $\bar{C}_{\mathrm{P}}$ is calculated by

$$\bar{C}_{\mathrm{P}}=\frac{\frac{1}{t}\int_0^t\left(\sum_s -\boldsymbol{H}(\boldsymbol{X}(s,t),t')\cdot\boldsymbol{u}(\boldsymbol{X}(s,t),t')\right)\mathrm{d}t'}{\frac{1}{2}\rho\boldsymbol{u}_\infty^3 D}\tag{17}$$

where $-\boldsymbol{H}$ is the local force exerted by the fish on the fluid; $\boldsymbol{u}$ the velocity of the fish and it can be set using the *Kármán* gait analytical model.

3 Results and Discussion

3.1 Numerical validation

To verify the present calculational model, we perform the simulation of the uniform flow past a stationary circular cylinder without foil behind the cylinder. As a benchmark case, this flow has been investigated based on other numerical schemes[32, 34, 42]. The comparison between the calculation results of the present method and the numerical results from the existing literature can serve as the verification of this method. The computational domains of $40D\times40D$ is used, and the center of the cylinder is positioned at ($20D$, $20D$). The uniform mesh is applied into the entire computational domain benefiting from excellent parallelism properties of IB-LBM. The lattice density of $D=50\Delta x$ and the Lagrangian point density of $\Delta l=\frac{2}{3}\Delta x$ are used. The initial density ρ_0 and velocity u_0 are set to be 1.0 and (0.1, 0), respectively. The Re is calculated based on the inlet velocity U, D, and v, $Re=UD/v$.

The drag coefficient C_D and the lateral force coefficient C_L can be calculated using $C_D=F_D/(0.5\rho_0U^2D)$ and $C_L=F_L/(0.5\rho_0U^2D)$, where F_D and F_L are the x-direction and y-direction components of the total force acting on the surface of the cylinder. The dimensionless length L_w of recirculating wake is calculated by using $L_w=L/D$. The Strouhal Number S_t are calculated using $S_t=f_{vs}D/u_\infty$, where f_{vs} is the frequency of vortex shedding. As shown in Table 2, the agreement with the available results demonstrates the ability of the present model to predict the steady and unsteady flow evolution.

Table 2 Comparison of the available results and the present results for flow over a stationary cylinder at *Re*=20, 40, 100

Method	$Re=20$		$Re=40$		$Re=100$		S_t
	C_D	L_w	C_D	L_w	$\bar{C}_D$	C_L	
Ref.[32]	2.119	0.937	1.586	2.320	1.362	±0.341	0.162
Ref.[34]	2.091	0.930	1.565	2.310	1.364	±0.344	0.163
Ref.[42]	2.084	0.960	1.560	2.360	1.368	±0.346	0.162
The presented	2.112	0.975	1.580	2.375	1.385	±0.353	0.160

In order to further verify the validation of the present IB-LBM used to deal with the problem of the flow around the moving boundary, the simulation of a NACA0015 airfoil that heaves and pitches simultaneously in a uniform flow[43-44] is carried out. The pitching and heaving motion, $\theta(t)=\theta_0\sin(2\pi ft)$ and $H(t)=H_0\sin(2\pi ft+\pi/2)$, are forced by the IB model at $Re=1\ 100$ and $H_0=L_f$, where H_0 is the heaving amplitude; θ_0 the pitching amplitude; and L_f the chord length of the airfoil. The simulations with the same numerical parameters used by Kinsey et al.[43] and Wu et al.[44] are performed, and two set of parameters are set as: $\theta_0=76.33°$, $f^*=0.14$ and $\theta_0=60°$, $f^*=0.18$. The mean drag coefficient $\bar{C}_D$, the peak of the lift coefficient $\bar{C}_L$, and the power extraction efficiency η are listed in Table 3. The consistency between the current simulation results and the results of the existing literature[43-44] verifies that the present IB-LBM used in this work is suitable for the flow around a moving boundary.

Table 3 Parameters of the flows over an oscillating NACA0015 airfoil at *Re*=1 100, $H_0=L_f$, and $x_p=L/3$

Method	$\theta_0=76.33°, f^*=0.14$			$\theta_0=60°, f^*=0.18$		
	$\bar{C}_D$	$\bar{C}_L$	η	$\bar{C}_D$	$\bar{C}_L$	η
Ref.[43]	2.014	1.910	0.337	0.690	1.256	0.114
Ref.[44]	2.107	1.969	0.347	0.711	1.248	0.122
The presented	2.113	1.989	0.351	0.718	1.239	0.119

3.2 Fish swimming in the cylinder wake

In this work, based on the model shown in Fig.1, we study the hydrodynamic mechanism of fish exploiting vortex from the perspective of flow patterns. These experimental studies show that the hydrodynamic optimized properties of fish are related to the relative movement of the *Kármán* gait and the incoming vortices, and the relative movement is described using the phase difference φ.

In order to control the relative motion between the vortical flow produced by the upstream stationary cylinder and the downstream *Kármán* gait foil, we define the foil-vortex phase difference φ. First, the simulation of flow pass through a single stationary cylinder is performed to generate the stable vortex sheet wake at $Re=100$. When the vortical flow reaches a stable state, we use the obtained wake variables (the wake wavelength and the vortex shed frequency) to set the kinematic parameters of the *Kármán* gait model. Then, a stationary foil is placed behind the cylinder with the downstream distance $2L$. After the vortical flow reaches stable again, we take the state of the flow field where the minus vortex center ($\omega_z L/U<0$) arrives at the foil center as the initial state of the unsteady flow simulation. Last, the foil begins to perform the Kármán gait motion with the initial phase ϕ_0, and we define the foil-vortex phase difference φ of the simulation equal to ϕ_0.

To investigate the effect of φ on the periodic features of the hydrodynamic forces experienced by the swimming foil in the cylinder wake, a series of the simulations are performed under different φ conditions. Fig.3 shows the mean thrust coefficient as a function of the time series. In Fig.3, for most of the ten different φ, the $\bar{C}_T(T)$ curve is approximately a straight line, which implies that the flow evolution is periodic, because the surrounding fluid provides approximately equal propulsion to the fish in each kinematic cycle. T represents the vortex shedding period. On the contrary, the fluctuating and stronger resistances are captured at φ of 36° and 180°, which demonstrates that the fish cannot capture energy from the aperiodic flow inducted by the Kármán gait at such phase difference. We further conducted a series of simulations with subdivided φ around 36° and 180°. The results show that when φ is in the range of 27° to 45°, or 171° to 189°, the flow could provide aperiodic resistance for the fish. As a counterexample, these phase differences should be prevented in term of optimizing the propulsion system.

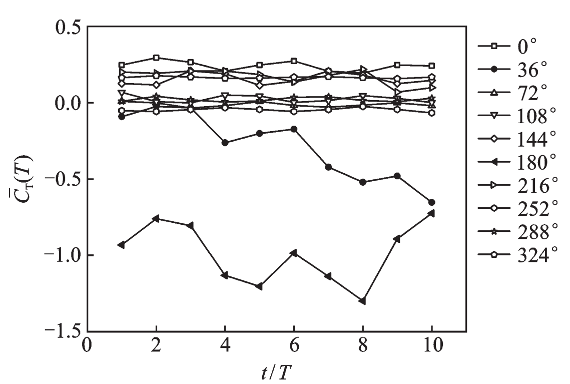

Fig.3 Cycle-by-cycle $\bar{C}_T(T)$ curves for φ of 0°, 36°, 72°, 108°, 144°, 180°, 216°, 252°, 288° and 324°

For the flow with the periodic feature, the propulsion performance and the locomotion cost are quantified using the mean thrust coefficient and the mean power coefficient for five oscillation cycles. Fig.4 shows $\bar{C}_T(5T)$ and $\bar{C}_P(5T)$ as a function of φ from 0° to 360°, excluding the interval from 27° to 45° and from 171° to 189°. In Fig.4(a), the dashed line represents the dividing line between thrust and resistance. We observe that the maximum thrust is obtained at φ of 0° and 198°, whereas the strongest resistance is encountered at φ of 54° and 252°. On the other hand, the minimum power cost is needed at φ of 18° and 216° while at φ of 108° and 288° the maximal power cost is required to hold the Kármán gait. From the perspective of propulsion system design, it is desirable to achieve greater propulsion based on less energy consumption, which shows that the relative movement mode with larger energy consumption must be prevented. At φ of 0°, the hydrodynamic performance of the fish is desirable. We assume that the Kármán gait with φ of 0° is the real locomotion mode taken by fish in the wake of Kármán vortex streets. The discussion on the hydrodynamic mechanisms of fish exploiting vortices will be carried out under φ of 0° condition.

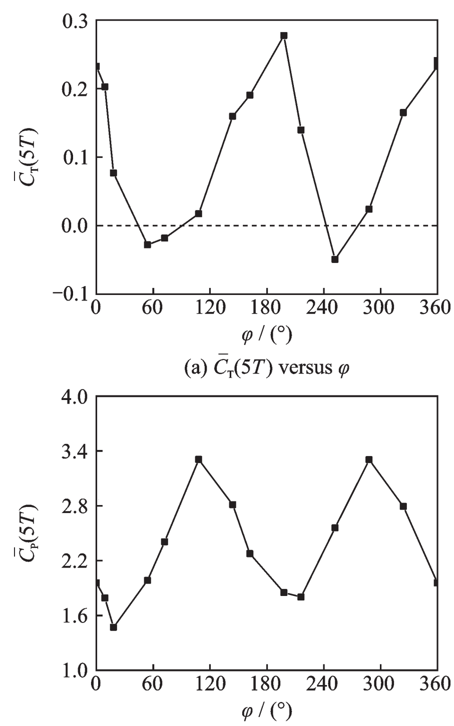

Fig.4 The mean thrust and power coefficient for φ of 0°, 36°, 72°, 108°, 144°, 180°, 216°, 252°, 288° and 324°

As the reference case, we conduct a simulation with the fixed fish holding station behind the cylinder at Re=100. Temporal thrust and lateral force coefficient for the two cases are illustrated in Fig.5. For the fixed fish, the fish will encounter resistance almost in a whole cycle time. This result explains why the fixed fish hardly obtains propulsion from the flow. For the swimming fish, the amplitude of thrust curve is amplified, and the fish captures thrust from the flow for most of the cycle time, which results in the maximum mean thrust coefficient. In Fig.5(b), for the two cases, the nature of temporal lateral force coefficient curves is almost the same, except for their phase. This could cause that the Kármán gait has the same mean lateral force to the fixed fish. These results imply that the Kármán gait aids the fish to obtain the optimal propulsion performance, but its effect on the lateral force is weak.

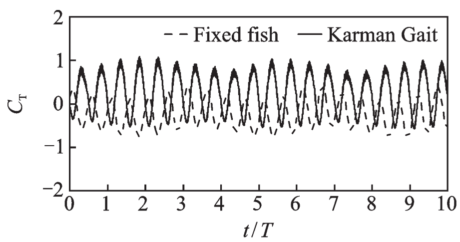

(a) Time history of C_T for the fixed fish and the fish adopting the Kármán Gait with φ of 0°

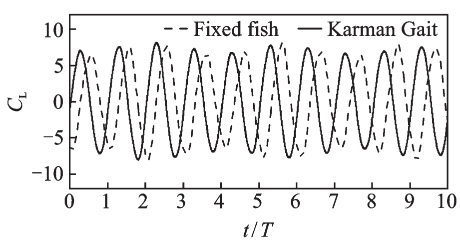

(b) Time history of C_L for the fixed fish and the fish adopting the Kármán Gait with φ of 0°

Fig.5 Time histories of C_T and C_L for the fixed fish and the fish adopting the Kármán gait with φ of 0°

The time-series of the Kármán gait and instantaneous vortex distribution around the fish are plotted in Fig.6. We define the incoming vortex acting on the fish as "vortex 1". The downward locomotion of the fish head causes significant splitting of a kinematic vortex, which locates on the upper side of the body. The generation of vortex is ending when the lowest position of lateral translation is reached, and the upward motion of the fish head begins. The

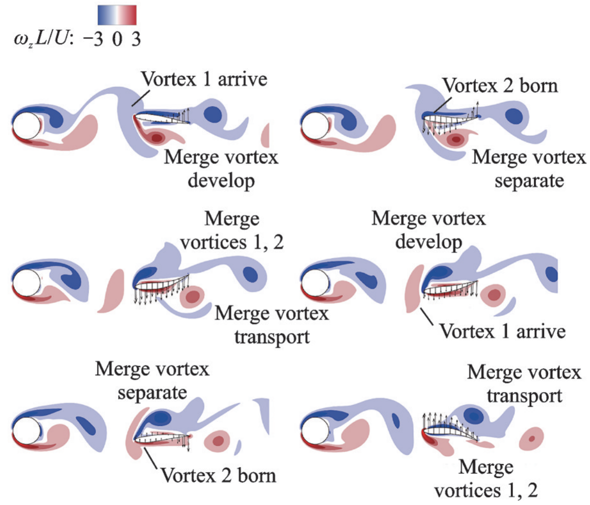

Fig.6 Instantaneous vortex distribution around the fish in one kinematic cycle for φ of 0°

upward motion of the fish head creates an inverted kinematic vortex on the underside of the body. The two counter-rotating kinematic vortices are called "vortex 2". The same formation is done by the caudal fin, and a pair of counter-rotating kinematic vortices are produced (called "vortex 3"). It can be observed that the relative movement of the fish locomotion and the incoming vortices is consistent with the experimental results of Liao[23].

To understand the reason why the optimized propulsion performance is obtained, we perform Fourier spectral analysis to study the intrinsic nature of unsteady hydrodynamic force. As shown in Fig.7, the distributions of fundamental harmonics both for C_D and C_L are like the two cases. The frequency of the kinematic vortices induced by the Kármán gait is equal to the frequency of the incoming vortices. The major difference is the amplitude of the fundamental harmonics. Moreover, the contribution of the subharmonics is cut in the spectrum of C_D. For the fixed fish, the amplitude of the fundamental harmonics is related to the intensity carried by the incoming vortices. Therefore, for the swimming fish, the larger amplitude demonstrates that the intensity of incoming vortices has increased. This may also explain why the frequency of the Kármán gait is adjusted to be equal to the frequency of the Kármán vortex street. Considering the characteristics of Fig.6 and Fig.7, we believe that under

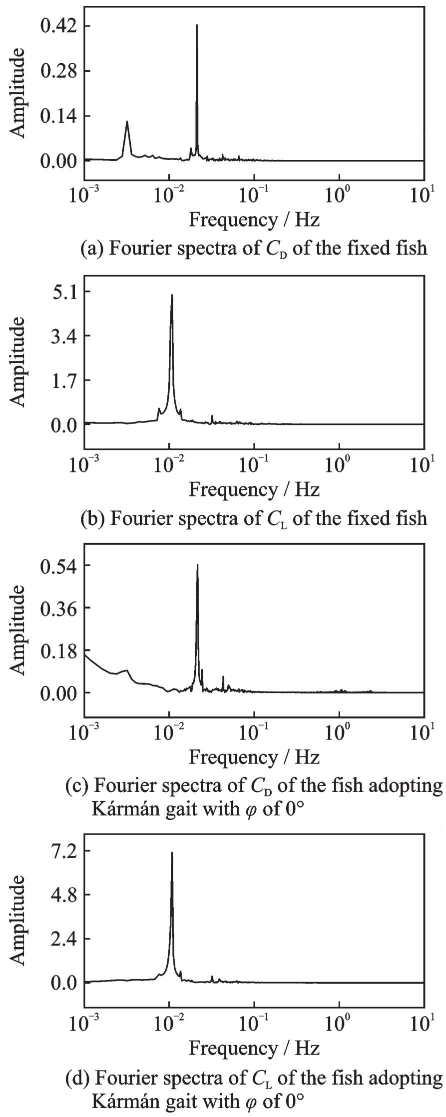

(a) Fourier spectra of C_D of the fixed fish

(b) Fourier spectra of C_L of the fixed fish

(c) Fourier spectra of C_D of the fish adopting Kármán gait with φ of 0°

(d) Fourier spectra of C_L of the fish adopting Kármán gait with φ of 0°

Fig.7 Fourier spectra of C_D and C_L of the fixed fish and the fish adopting the Kármán gait with φ of 0°

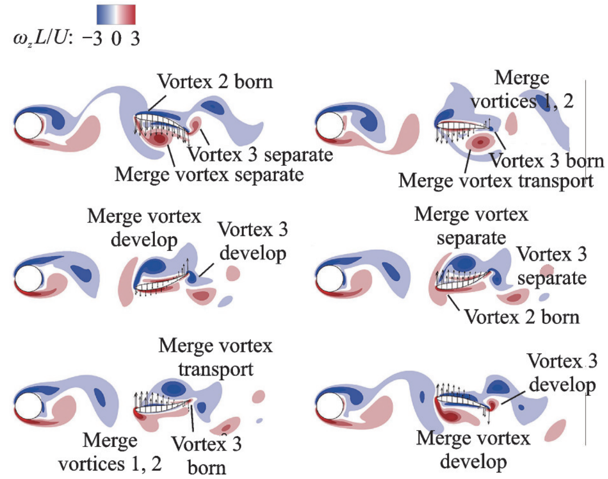

Fig.8 Instantaneous vortex distribution around the fish in one kinematic cycle for φ of 54°

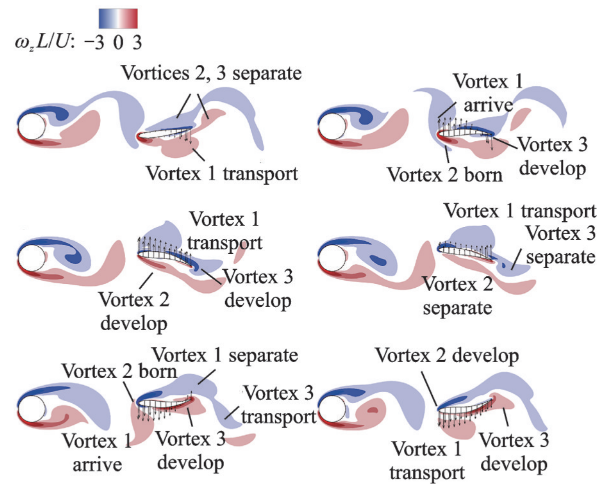

Fig.9 Instantaneous vortex distribution around the fish in one kinematic cycle for φ of 108°

the conditions of the same rotation direction and frequency, "vortex 2" enhances the energy carried by "vortex 1", and "merged vortex" is derived from the enhanced "vortex 1".

We further plot the Kármán gait and instantaneous vortex distribution around the fish at φ of 54° and 180° in Fig.8 and Fig.9, respectively, to illustrate the origin of resistance. In Fig.8, the main discrepancy is that the fishtail moves away from the "merged vortex" when the "merged vortex" slides near the fishtail. This process shows that a pair of stronger "vortex 3" can be generated. This means that the tendency of the fishtail to move toward the "merged vortex" plays a key role in the process of fish exploiting vortices, but this role is negative.

In addition, in Fig.9, we see that the vibration of the fish head produces "vortex 2", and its direction of rotation is opposite to "vortex 1". From the mean thrust coefficient mentioned above (in Fig.3), we infer that "vortex 2" with opposite direction of rotation to that of "vortex 1" will disturb the periodic properties of flow evolution, thus the fish cannot extract energy from the drifting vortex.

Last, the contribution of the four components of Kármán gait on fish swimming performance is assessed. The locomotion is demonstrated by utilizing the four traveling wave equations in the wake of the cylinder at $Re=100$. The fixed fish and the Kármán gait with φ of 0° are considered as the two comparisons. We also calculate $\bar{C}_T(5T)$ and $\bar{C}_P(5T)$ for each motion in Table 4. From the results (see

Fig.10), we conclude that propulsion mainly originates from lateral translation. However, it requires a greater energy consumption to hold the locomotion. Rotation, undulation, and head motions cooperate with each other to reduce energy consumption of lateral translation motion. Therefore, hydrodynamic performance in fish swimming combines high propulsion and the desired locomotion cost. Four components work together to help fish achieve the desired hydrodynamic performance.

Table 4 $\bar{C}_T(5T)$ and $\bar{C}_P(5T)$ for different states

State	$\bar{C}_T(5T)$	$\bar{C}_P(5T)$
Stationary	−0.191	—
Kármán gait	0.232	1.954
Translation	0.259	2.491
Rotation	−0.112	0.117
Undulation	−0.323	1.135
Head	−0.206	−0.021

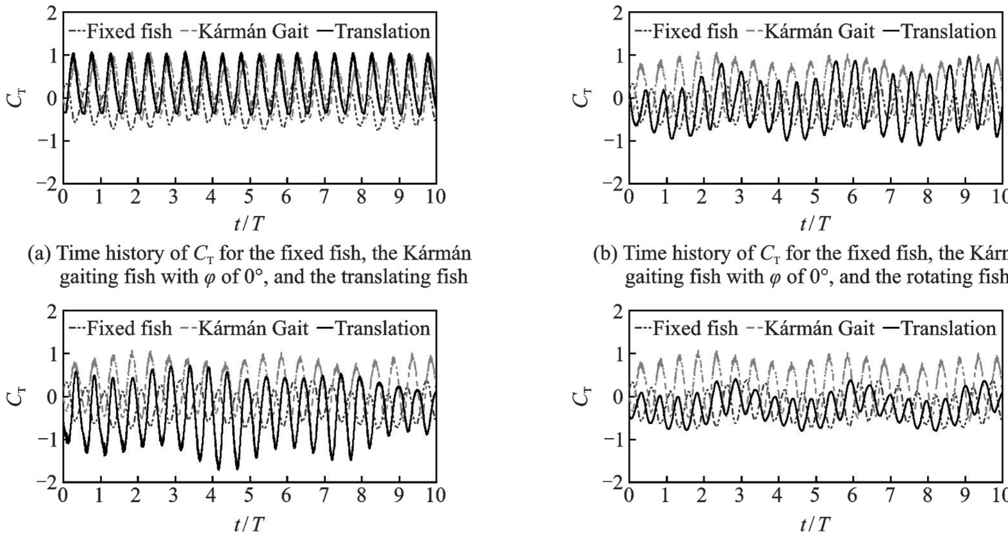

(a) Time history of C_T for the fixed fish, the Kármán gaiting fish with φ of 0°, and the translating fish

(b) Time history of C_T for the fixed fish, the Kármán gaiting fish with φ of 0°, and the rotating fish

(c) Time history of C_T for the fixed fish, the Kármán gaiting fish with φ of 0°, and the undulatory fish

(d) Time history of C_T for the fixed fish, the Kármán gaiting fish with φ of 0°, and the heading fish

Fig.10 Time histories of C_T for translation, rotation, undulation and head motion and the fixed fish and the Kármán gait as two comparisons

4 Conclusions

Based on IB-LBM, a flow solver that flexibly copes with complex deformable moving boundaries and controls the computational cost is developed to solve the problems of fish swimming in the vortex environment. Controlling the Kármán vortex street and the fish locomotion to model the nonlinear dynamic system, the hydrodynamic mechanism of the fish exploiting vortices to improve their swimming performance is discussed in terms of propulsion and energy consumption. Numerical results illustrate the reason for the experimental conclusion that the fish adjusts the frequency of vibration to the frequency of the incoming vortex is that the moving vortex with the same frequency and rotation direction induced by the fish head will enhance the intensity of the incoming vortex. The movement tendency of the fish tail towards the "merged vortex" determines the fish to extract energy from the vortex. Four components of the Kármán gait locomotion work together to help fish obtain the optimized propulsion based on a desired energy consumption.

The proposed flow solution only involves the effect of the deformable boundary on the flow evolution, that is, the moving boundary is actively controlled by the kinematics analytical model. For fluid-structure interaction dynamics, the effect of hydrodynamic force on the fish locomotion should be considered. In future work, we will develop a flow solution model that considers the influence of hydrodynamic force on the kinematic model of fish, and anticipate to provide insights for engineering applications.

References

[1] LI Lijun, LI Gen, LI Ruoxin, et al. Multi-fin kinematics and hydrodynamics in pufferfish steady swimming[J]. Ocean Engineering, 2018, 158: 111-122.

[2] KRISHNADAS A, RAVICHANDRAN S, RAJAGOPAL P. Analysis of biomimetic caudal fin shapes for optimal propulsive efficiency[J]. Ocean Engineering, 2018, 153: 132-142.

[3] BERGMANN M, IOLLO A. Bioinspired swimming simulations[J]. Journal of Computational Physics, 2016, 323: 310-321.

[4] KHALID M S U, AKHTAR I, IMTIAZ H, et al. On the hydrodynamics and nonlinear interaction between fish in tandem configuration[J]. Ocean Engineering, 2018, 157: 108-120.

[5] XIAO Qing, SUN Ke, LIU Hao, et al. Computational study on near wake interaction between undulation body and a D-section cylinder[J]. Ocean Engineering, 2011, 38(4): 673-683.

[6] LI Chao, YANG Wenjing, XU Xinhai, et al. Numerical investigation of fish exploiting vortices based on the *Kármán* gaiting model[J]. Ocean Engineering, 2017, 140: 7-18.

[7] TAYLOR G I. Analysis of the swimming of microscopic organisms[J]. Proceedings of the Royal Society of London: Series A, Mathematical and Physical Sciences, 1951, 209(1099): 447-461.

[8] LIGHTHILL M J. Note on the swimming of slender fish[J]. Journal of Fluid Mechanics, 1960, 9(2): 305-317.

[9] CHENG Jianyu, ZHUANG Lixian, TONG Binggang. Analysis of swimming three-dimensional waving plates[J]. Journal of Fluid Mechanics, 1991, 232: 341-355.

[10] LIGHTHILL M J. On the Weis-Fogh mechanism of lift generation[J]. Journal of Fluid Mechanics, 1973, 60(1): 1-17.

[11] JONES K D, DOHRING C M, PLATZER M F. Experimental and computational investigation of the Knoller-Betz effect[J]. AIAA Journal, 1998, 36(7): 1240-1246.

[12] GOPALKRISHNAN R, TRIANTAFYLLOU M S, TRIANTAFYLLOU G S, et al. Active vorticity control in a shear flow using a flapping foil[J]. Journal of Fluid Mechanics, 1994, 274: 1-21.

[13] AKHTAR I, MITTAL R, LAUDER G V, et al. Hydrodynamics of a biologically inspired tandem flapping foil configuration[J]. Theoretical and Computational Fluid Dynamics, 2007, 21(3): 155-170.

[14] KARBASIAN H R, ESFAHANI J A. Enhancement of propulsive performance of flapping foil by fish-like motion pattern[J]. Computers & Fluids, 2017, 156: 305-316.

[15] BARRETT D S, TRIANTAFYLLOU M S, YUE D K P, et al. Drag reduction in fish-like locomotion[J]. Journal of Fluid Mechanics, 1999, 392: 183-212.

[16] BEAL D N, HOVER F S, TRIANTAFYLLOU M S, et al. Passive propulsion in vortex wakes[J]. Journal of Fluid Mechanics, 2006, 549: 385-402.

[17] SHAO Xueming, PAN Dingyi, DENG Jian, et al. Hydrodynamic performance of a fish-like undulating foil in the wake of a cylinder[J]. Physics of Fluids, 2010, 22(11): 111903.

[18] BERGMANN M, IOLLO A. Modeling and simulation of fish-like swimming[J]. Journal of Computational Physics, 2011, 230(2): 329-348.

[19] ZHU Y, TIAN F B, YOUNG J, et al. A numerical study of fish adaption behaviors in complex environments with a deep reinforcement learning and immersed boundary-lattice Boltzmann method[J]. Scientific Reports, 2021, 11(1): 1-20.

[20] AKANYETI O, LIAO J C. A kinematic model of *Kármán* gaiting in rainbow trout[J]. Journal of Experimental Biology, 2013, 216(24): 4666-4677.

[21] LIAO J C, BEAL D N, LAUDER G V, et al. The *Kármán* gait: Novel body kinematics of rainbow trout swimming in a vortex street[J]. Journal of Experimental Biology, 2003, 206(6): 1059-1073.

[22] LIAO J C. Neuromuscular control of trout swimming in a vortex street: Implications for energy economy during the Karman gait[J]. Journal of Experimental Biology, 2004, 207(20): 3495-3506.

[23] LIAO J C. A review of fish swimming mechanics and behaviour in altered flows[J]. Philosophical Transactions of the Royal Society B: Biological Sciences, 2007, 362(1487): 1973-1993.

[24] STEWART W J, TIAN F B, AKANYETI O, et al. Refuging rainbow trout selectively exploit flows behind tandem cylinders[J]. Journal of Experimental Biology, 2016, 219(14): 2182-2191.

[25] TONG Ying, XIA Jian, CHEN Long, et al. An immersed boundary lattice Boltzmann method based on implicit diffuse direct-forcing scheme[J]. Chinese Journal of Theoretical and Applied Mechanics, 2022, 54(1): 94-105. (in Chinese)

[26] MITTAL R, IACCARINO G. Immersed boundary methods[J]. Annu Rev Fluid Mech, 2005, 37:

239-261.

[27] HUANG Weixi, TIAN Fangbao. Recent trends and progress in the immersed boundary method[J]. Proceedings of the Institution of Mechanical Engineers Part C: Journal of Mechanical Engineering Science, 2019, 233(23/24): 7617-7636.

[28] FENG Z G, MICHAELIDES E E. The immersed boundary-lattice Boltzmann method for solving fluid-particles interaction problems[J]. Journal of Computational Physics, 2004, 195(2): 602-628.

[29] FENG Z G, MICHAELIDES E E. Proteus: A direct forcing method in the simulations of particulate flows[J]. Journal of Computational Physics, 2005, 202(1): 20-51.

[30] DUPUIS A, CHATELAIN P, KOUMOUTSAKOS P. An immersed boundary-lattice-Boltzmann method for the simulation of the flow past an impulsively started cylinder[J]. Journal of Computational Physics, 2008, 227(9): 4486-4498.

[31] YUAN Haizhuang, NIU Xiaodong, SHU Shi, et al. A momentum exchange-based immersed boundary-lattice Boltzmann method for simulating a flexible filament in an incompressible flow[J]. Computers & Mathematics with Applications, 2014, 67(5): 1039-1056.

[32] DASH S M. A flexible forcing immersed boundary-simplified lattice Boltzmann method for two and three-dimensional fluid-solid interaction problems[J]. Computers & Fluids, 2019, 184: 165-177.

[33] SHU C, LIU N, CHEW Y T. A novel immersed boundary velocity correction-lattice Boltzmann method and its application to simulate flow past a circular cylinder[J]. Journal of Computational Physics, 2007, 226(2): 1607-1622.

[34] WU J, SHU C. Implicit velocity correction-based immersed boundary-lattice Boltzmann method and its applications[J]. Journal of Computational Physics, 2009, 228(6): 1963-1979.

[35] GUO Zhaoli, ZHENG Chugang, SHI Baochang. Discrete lattice effects on the forcing term in the lattice Boltzmann method[J]. Physical Review E, 2002, 65(4): 046308.

[36] HE X Y, CHEN S Y, DOOLEN G D. A novel thermal model for the lattice Boltzmann method in incompressible limit[J]. Journal of Computational Physics, 1998, 146(1): 282-300.

[37] STERLING J D, CHEN S Y. Stability analysis of lattice Boltzmann methods[J]. Journal of Computational Physics, 1996, 123(1): 196-206.

[38] SHAN Xiaowen, YUAN Xuefeng, CHEN Hudong. Kinetic theory representation of hydrodynamics: A way beyond the Navier-Stokes equation[J]. Journal of Fluid Mechanics, 2006, 550: 413-441.

[39] QIAN Y D, D'HUMIÈRES D, LALLEMAND P. Lattice BGK models for Navier-Stokes equation[J]. EPL (Europhysics Letters), 1992, 17(6): 479.

[40] YANG Xiaolei, ZHANG Xing, LI Zhilin, et al. A smoothing technique for discrete delta functions with application to immersed boundary method in moving boundary simulations[J]. Journal of Computational Physics, 2009, 228(20): 7821-7836.

[41] DASH S M, LEE T S, LIM T T, et al. A flexible forcing three dimension IB-LBM scheme for flow past stationary and moving spheres[J]. Computers & Fluids, 2014, 95: 159-170.

[42] KANG S K, HASSAN Y A. A comparative study of direct-forcing immersed boundary-lattice Boltzmann methods for stationary complex boundaries[J]. International Journal for Numerical Methods in Fluids, 2011, 66(9): 1132-1158.

[43] KINSEY T, DUMAS G. Parametric study of an oscillating airfoil in a power-extraction regime[J]. AIAA Journal, 2008, 46(6): 1318-1330.

[44] WU J, QIU Y L, SHU C, et al. Pitching-motion-activated flapping foil near solid walls for power extraction: A numerical investigation[J]. Physics of Fluids, 2014, 26(8): 083601.

Acknowledgements This work was supported by the Priority Academic Program Development of Jiangsu Higher Education Institutions (PAPD). The authors realize that the time available for a review of such an ambitious subject are limited and, thus, regretfully, we are unable to cover many important contributions. The authors would like to acknowledge the following people for their assistance: GAO He, YANG Limin, and LI Longfei. They are members of the Key Laboratory of Unsteady Aerodynamics and Flow Control of Ministry of Industry and Information Technology, Nanjing University of Aeronautics and Astronautics.

Authors Ms. **TONG Ying** is a Ph.D. candidate in the Department of Aerodynamics, Nanjing University of Aeronautics and Astronautics (NUAA), majoring in fluid mechanics. Her research areas include computational fluid dynamics, immersed boundary lattice Boltzmann method, bionic propulsion, and fluid-structure interaction dynamics.

Prof. **XIA Jian** received his B.S. and Ph.D. degrees in aerospace engineering from NUAA, Nanjing, China, in 1992 and 1998, respectively. He worked as a post-doctoral researcher in College of Mechanical and Aerospace Engineering at University of California Irvine and a visiting scholar at the University of Texas at Arlington before assuming his current position at NUAA. His research areas include computational fluid dynamics, fluid-structure interaction, aerodynamic optimization design, and calculate aeroacoustics.

Author contributions Ms. TONG Ying designed the study, conducted the analysis, interpreted the results, and wrote the manuscript. Prof. XIA Jian contributed to the discussion and background of the study. Dr. CHEN Long complied the models. Mr. XUE Haotian contributed to the literature collection and data post-processing. All authors commented on the manuscript draft and approved the submission.

Competing interests The authors declare no competing interests.

(Production Editor:ZHANG Bei)

圆柱尾流与游鱼间相互作用的数值计算研究

佟 莹[1,2],夏 健[1,2],陈 龙[1,2],薛浩天[1,2]

(1.南京航空航天大学航空学院,南京 210016,中国;

2.南京航空航天大学非定常空气动力学与流动控制工业和信息化部重点实验室,南京 210016,中国)

摘要:为了预测鱼类游泳问题的流动演变,开发了一种基于浸入边界格子玻尔兹曼方法的流动求解器。采用基于隐式边界力校正框架的灵活迭代算法降低计算成本和内存。在确定边界节点的速度修正后动量力由简单的直接力公式描述,无需复杂的积分计算。使用所提出的流动求解器,分析了鱼引起的动态失速涡与非定常流动中的传入涡之间的流体动力学相互作用。数值模拟结果揭示了鱼类利用涡流增强自身水动力性能的机制。优越的游泳性能源于"合并涡流"与鱼尾运动之间的相对运动,相互作用由相位差控制。"合并涡"的形成条件成为鱼类利用涡流提高游泳性能的关键因素。进一步讨论了运动主要成分的影响。根据数值模拟结果得出结论,横向平移在推进中起着至关重要的作用,而与旋转和头部运动相结合的身体起伏降低了运动成本。

关键词:浸没边界;格子Boltzmann方法;可变形动边界;流体-游鱼相互作用;水动力机制;仿生推进